The Astrophysical Journal, 962:61 (9pp), 2024 February 10 https://doi.org/10.3847/1538-4357/ad1758

On the Maximum Mass and Oblateness of Rotating Neutron Stars with Generic Equations of State

Carlo Musolino[1], Christian Ecker[1], and Luciano Rezzolla[1,2,3]
[1] Institut für Theoretische Physik, Goethe Universität, Max-von-Laue-Straße 1, D-60438 Frankfurt am Main, Germany
[2] School of Mathematics, Trinity College, Dublin 2, Ireland
[3] Frankfurt Institute for Advanced Studies, Ruth-Moufang-Str. 1, D-60438 Frankfurt am Main, Germany
Received 2023 July 17; revised 2023 December 14; accepted 2023 December 18; published 2024 February 7

Abstract

A considerable effort has been dedicated recently to the construction of generic equations of state (EOSs) for matter in neutron stars. The advantage of these approaches is that they can provide model-independent information on the interior structure and global properties of neutron stars. Making use of more than 10^6 generic EOSs, we assess the validity of quasi-universal relations of neutron-star properties for a broad range of rotation rates, from slow rotation up to the mass-shedding limit. In this way, we are able to determine with unprecedented accuracy the quasi-universal maximum-mass ratio between rotating and nonrotating stars and reveal the existence of a new relation for the surface oblateness, i.e., the ratio between the polar and equatorial proper radii. We discuss the impact that our findings have on the imminent detection of new binary neutron-star mergers and how they can be used to set new and more stringent limits on the maximum mass of nonrotating neutron stars, as well as to improve the modeling of the X-ray emission from the surface of rotating stars.

Unified Astronomy Thesaurus concepts: Neutron stars (1108); General relativity (641); Pulsars (1306); Gravitation (661); Fundamental parameters of stars (555); Nuclear astrophysics (1129)

1. Introduction

Matter inside neutron stars is compressed by gravity to densities a few times larger than the saturation density of atomic nuclei, $n_s = 0.16\,\mathrm{fm}^{-3}$, making them the most compact material objects known in the Universe. In principle, the properties of neutron stars are fully determined by the equation of state (EOS) of dense and cold, neutron-rich baryonic and possibly quark matter. In practice, however, because the EOS is known only with large uncertainties, our knowledge of even the most basic properties suffers from serious limitations that are only mildly mediated by astronomical observations and laboratory experiments. Among the various properties of neutron stars for any given EOS, the maximum masses $M_{\rm max}$ of rotating and $M_{\rm TOV}$ of nonrotating configurations (TOV for Tolman–Oppenheimer–Volkoff) bear particular significance both in gravity and in nuclear physics.

Direct measurements of mass and radius set strict lower limits on the maximum mass of neutron stars $M_{\rm TOV} \gtrsim 2\,M_\odot$ (Fonseca et al. 2021) and constrain their radii to $\simeq$11–14 km (Miller et al. 2021; Riley et al. 2021). Additional upper bounds on neutron-star radii and tidal deformabilities have been deduced from the first direct gravitational-wave detection of a binary neutron-star merger GW170817 by the LIGO and Virgo collaborations (The LIGO Scientific Collaboration et al. 2019). From this event, upper bounds on the maximum mass $M_{\rm TOV} \lesssim 2.33\,M_\odot$ have been derived from the associated gamma-ray burst GRB 170817A (Margalit & Metzger 2017; Rezzolla et al. 2018a; Ruiz et al. 2018; Shibata et al. 2019).

One of the reasons why accurate theoretical predictions of neutron-star properties are difficult is that reliable calculations of the EOS are currently only available from chiral effective field theory at densities $n_b \lesssim n_s$ (see, e.g., Hebeler et al. 2013; Gandolfi et al. 2019; Drischler et al. 2020; Keller et al. 2021) and in the opposite limit from pQCD (see, e.g., Freedman & McLerran 1977; Vuorinen 2003; Gorda et al. 2021a, 2021b) at densities $n_b \gtrsim 40\,n_s$, which are much larger than those reached inside neutron stars (see also Komoltsev & Kurkela 2022). Between these limits, the only available options are either to build models that reproduce the expected behavior of QCD (see, e.g., Beloin et al. 2019; Traversi et al. 2020; Bastian 2021; Jie et al. 2021; Demircik et al. 2022; Ivanytskyi & Blaschke 2022, for some recent attempts) or to construct agnostic (model-independent) parameterizations for the EOS and constrain them with astronomical or multimessenger measurements.

Our incomplete knowledge of the EOS is partially compensated by a number of quasi-universal, i.e., essentially EOS-independent, relations that have been found among certain neutron-star quantities over the years, in terms of both isolated rotating and nonrotating stars (see, e.g., Yagi & Yunes 2013; Chakrabarti et al. 2014; Doneva et al. 2014; Haskell et al. 2014; Pappas & Apostolatos 2014; Breu & Rezzolla 2016; Weih et al. 2018; Konstantinou & Morsink 2022; Nath et al. 2023) and the gravitational-wave signal from binary systems (see, e.g., Bauswein & Janka 2012; Read et al. 2013; Bernuzzi et al. 2014; Takami et al. 2015; Rezzolla & Takami 2016; Bauswein et al. 2019; Most et al. 2019; Weih et al. 2020; Gonzalez et al. 2023); see Yagi & Yunes (2017) for a review. Clearly, the robustness of these quasi-universal relations depends on the number of EOSs that are employed in determining the relations. So far, the identification and study of quasi-universal relations has often been limited by the relatively small number of available models. At the same time, a growing number of recent works have explored the possibility of building very large sets of EOSs that satisfy all known theoretical and observational constraints and cover the

physically allowed space of EOSs (Landry & Essick 2019; Annala et al. 2020) and of related quantities, such as the sound speed (Altiparmak et al. 2022; Gorda et al. 2023a; Ecker & Rezzolla 2023) or the conformal anomaly (Annala et al. 2023; Brandes et al. 2023; Marczenko et al. 2023). These EOSs are built using either generic piecewise polytropes (see, e.g., Read et al. 2009; Kurkela et al. 2014; Lattimer & Steiner 2014; Tews et al. 2018a, 2018b; Most et al. 2018; Steiner et al. 2018), a parameterization of the sound speed (see, e.g., Annala et al. 2020; Altiparmak et al. 2022; Ecker & Rezzolla 2023) or nonparametric Gaussian process regression (see, e.g., Landry & Essick 2019; Gorda et al. 2023a, 2023b).

The purpose of this work is to exploit such large ensembles of generic EOSs to revisit the validity of quasi-universal relations of isolated slowly and rapidly rotating stars, and to study how the results depend on input from pQCD and on recently measured bounds.

2. Quasi-universal Relations

Among the quasi-universal relations found for isolated stars, one is particularly relevant for its impact on the stability of stellar models and was first discussed by Breu & Rezzolla (2016, BR16 hereafter). More specifically, using a relatively small number of 28 tabulated EOSs, BR16 pointed out that the critical mass $M_{\rm crit}$, that is, the mass of uniformly rotating neutron stars on the turning-point line (hereafter, the "critical line"), can be expressed in a quasi-universal relation through the specific angular momentum $j_{\rm crit}$ and that at the mass-shedding limit $j_{\rm Kep}$ along the critical line ($j_{\rm crit}$ and $j_{\rm Kep}$ are also denoted $\chi_{\rm crit}$ and $\chi_{\rm Kep}$, respectively; Most et al. 2020):

$$\frac{M_{\rm crit}}{M_{\rm TOV}} = 1 + a_2\left(\frac{j_{\rm crit}}{j_{\rm Kep}}\right)^2 + a_4\left(\frac{j_{\rm crit}}{j_{\rm Kep}}\right)^4, \tag{1}$$

where $a_2 = 0.132$ and $a_4 = 0.071$ (Breu & Rezzolla 2016). A few remarks are worth making. First, expression (1) provides the stellar mass along the critical (or "turning-point") line (Friedman et al. 1988), that is, the line in the (M, n_c) plane along which $\partial M/\partial n_c|_J = 0$, where n_c is the central number density. Second, because the turning-point criterion is a sufficient criterion for dynamical instability, the importance of (1) is that it allows one to determine for any rotation rate the critical mass above which a dynamical instability would trigger the collapse to a rotating black hole. Third, when considering the maximum value allowed for the specific angular momentum, Equation (1) marks the maximum mass of stable uniformly rotating configurations, namely, $M_{\rm max} := M_{\rm crit}(j_{\rm crit} = j_{\rm Kep})$. Finally, because the turning-point criterion is only a sufficient but not a necessary criterion for dynamical instability, the maximum mass at the upper end of the dynamical-instability line is actually set by the upper end of the so-called "neutral-stability" line. Such a mass is normally slightly larger than $M_{\rm max}$ and is attained at somewhat smaller central densities (see Takami et al. 2011; Weih et al. 2018, for a discussion).

In practice, the quasi-universal relation (1) is most often used to relate the endpoints of the critical line via the ratio of the maximum masses of rotating and nonrotating configurations, namely,

$$\mathcal{R} := \frac{M_{\rm max}}{M_{\rm TOV}}. \tag{2}$$

Using Equation (1), BR16 estimated the mass ratio to be $\mathcal{R} = 1.203 \pm 0.022$, in rough agreement with cruder estimates obtained previously with a much smaller number of EOSs (Cook et al. 1994a, 1994b; Lasota et al. 1996); similar values have later been reported by Bozzola et al. (2019) (1.15–1.31), Demircik et al. (2021) ($1.227^{+0.031}_{-0.016}$) for EOSs with a phase transition, Khosravi Largani et al. (2022) (1.200 ± 0.02 [1.1085 ± 0.0055] and 1.212 ± 0.009 [1.0995 ± 0.0055]) for hadronic and hybrid hadron–quark equations of state in cold beta equilibrium [resp. with constant entropy per baryon $s = 3k_{\rm B}$ and lepton fraction $Y_l = 0.3$], and Jie et al. (2023) (1.20815) for EOSs with heavy baryons. In what follows, we assess the validity of Equations (1) and (2) and refine the quasi-universal behavior exploiting a set of more than 10^6 different EOSs[4] that cover the entire physically allowed space of EOSs consistent with constraints from dense-matter theory and neutron-star observations. EOSs having features typical of a phase transition, such as kinks and plateaus of the pressure as a function of the number density, are naturally included in our sample but they are statistically rare and hence have a minor impact on our results.

For the construction of our EOSs we follow the procedure presented in a number of previous works, where the interested reader can find additional details (Altiparmak et al. 2022; Ecker & Rezzolla 2022, 2023). What is relevant to recall here is that we construct the EOSs with a 10-segment parameterization of the sound speed in which we can either impose or not the pQCD constraints at $\sim 40 n_s$. From the astrophysics side, we impose constraints coming from measurements of pulsar radii by the NICER collaboration on J0740+6620 (Miller et al. 2021; Riley et al. 2021) and J0030+0451 (Miller et al. 2019; Riley et al. 2019) by rejecting EOSs for which $R_{2.0} < 10.75$ km or $R_{1.1} < 10.8$ km, where the subscript indicates the corresponding gravitational mass of nonrotating stars. In addition, we impose an upper bound on the binary tidal deformability $\tilde{\Lambda}$ as deduced from the LIGO/Virgo detection of GW170817 by rejecting all EOSs with $\tilde{\Lambda} > 720$ (low-spin prior) (The LIGO Scientific Collaboration et al. 2019) at a chirp mass $\mathcal{M}_{\rm chirp} = 1.186\, M_\odot$ for mass ratios $q > 0.73$. The constraints from these astrophysical observations are imposed as sharp cutoffs on the EOS ensemble, which, as shown by Jiang et al. (2023), leads to good agreement of the important central part of the PDF obtained from a more expensive Bayesian analysis. Finally, we impose a lower bound $M_{\rm TOV}^{(-)}$ on the maximum mass of nonrotating neutron stars ($M_{\rm TOV}$) by rejecting all models with $M_{\rm TOV}$ below a prescribed cutoff. Since this constraint has been shown to have a significant impact on the space of allowed EOSs (Ecker & Rezzolla 2023), we have explored different values for $M_{\rm TOV}^{(-)}$ to account for the uncertainties on this bound.

Once the EOS ensemble has been generated, the corresponding models for rotating stars are constructed with the RNS code (Stergioulas & Friedman 1995). In particular, we solve for

[4] Interestingly, already $\mathcal{O}(10^3)$ EOSs are sufficient to obtain results very similar to those from the full set of 10^6 EOSs. This is because the probability density functions (PDFs) converge very rapidly, as demonstrated in the Appendix.

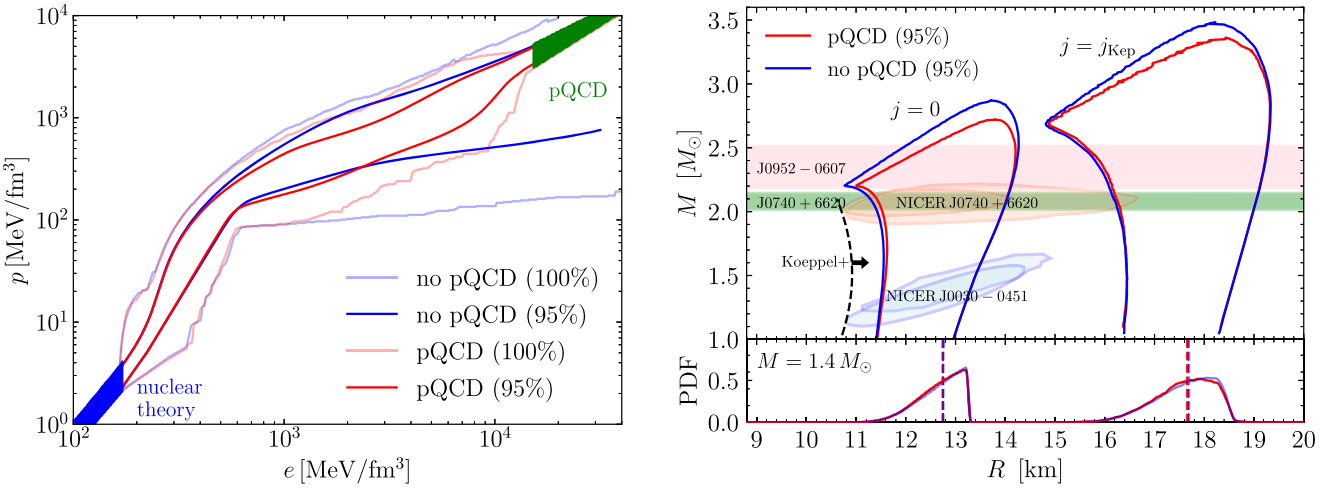

Figure 1. Left: 95% (dark colors) and 100% (light colors) confidence-level contours for an ensemble of 10^6 EOSs with $M_{\rm TOV}^{(-)} = 2.2\,M_\odot$, for which the pQCD constraints are imposed (red) or not (blue). Right: corresponding 95% confidence-level contours for the mass–radius relations of nonrotating stars ($j = 0$) and stars rotating at the mass-shedding frequency ($j = j_{\rm Kep}$; in this case the equatorial proper radii are used). Shaded areas indicate the imposed astrophysical constraints or the limits from the threshold mass to collapse (Koeppel et al. 2019); the bottom panel reports slices of the PDFs at $M = 1.4\,M_\odot$.

stationary and axisymmetric equilibrium solutions of uniformly rotating perfect fluids with varying central densities along sequences of constant angular momentum between $J = 0$ and $J = J_{\rm Kep}$, where $J_{\rm Kep}$ is the Keplerian (or "mass-shedding") angular momentum and is a function of n_c (see also Konstantinou & Morsink 2022; Jie et al. 2023, for similar analyses with a much smaller set of EOSs). The set of stellar models having $J = J_{\rm Kep}$ is also referred to as the Keplerian limit because along this sequence the angular velocity is the largest possible; any increase in the angular momentum at constant central density would lead to a shedding of mass at the equator. The endpoint of the Keplerian sequence marks the maximum mass at a Keplerian frequency, $M_{\rm max,\,Kep}$, and this is close to, but systematically larger than $M_{\rm max}$. The relative difference between the two masses is rather small, i.e., $M_{\rm max,Kep}/M_{\rm max} - 1 \lesssim 10^{-2}$, and therefore often ignored (e.g., Annala et al. 2022), but it is conceptually important that the two masses are kept distinct, as is done here.

The left panel of Figure 1 reports the 95% (dark lines) and 100% (light lines) confidence-level contours for our ensemble of 10^6 EOSs with $M_{\rm TOV}^{(-)} = 2.2\,M_\odot$ when the pQCD constraints are imposed (red) or not (blue). The right panel, on the other hand, shows the corresponding 95% confidence-level contours for the mass–radius relations of nonrotating stars ($j = 0$) and stars rotating at the mass-shedding limit ($j = j_{\rm Kep}$); in the rotating case, the equatorial radii are employed (see Appendix).

3. Results

Making use of our ensemble of 10^6 EOSs, we have constructed more than 10^8 nonrotating and rotating stellar models up to the mass-shedding limit. In this way, we have reconsidered several quasi-universal relations governing the properties of neutron stars and we first present the outcome of this analysis for the mass-ratio relation (1). In Figure 2 we show results for two different ensembles where the pQCD constraints are either imposed (red colors) or not (blue colors). In both cases, we use a lower bound of $M_{\rm TOV} > 2.2\,M_\odot$ to ensure consistency with the 1σ confidence interval for the direct mass measurement of the black-widow binary pulsar PSR J0952-0607 ($2.35 \pm 0.17\,M_\odot$) (Romani et al. 2022). More specifically, the colored areas in the (large) left panel of Figure 2 show the (95%) confidence intervals of the PDF with (red) and without (blue) imposing the pQCD constraint, while the solid lines of corresponding color mark the medians of the distributions. The median values and the corresponding confidence intervals of the distributions are still well approximated by expression (1), where we use a_2 and $\mathcal{R}$ as fitting parameters, thus fixing $a_4 = \mathcal{R} - (a_2 + 1)$; the best-fit coefficients are listed in Table 1 of the Appendix. Interestingly, the quadratic term in (1) provides a very good approximation up to $j \sim 0.7 j_{\rm Kep}$ and the quartic contribution becomes essential only for larger values of j.

Overall, we find that the new and much larger set of EOSs again shows a quasi-universal behavior similar to that proposed by BR16, as reported with a black solid line in Figure 2. The variance of the new universal relations is slightly larger than what was found by BR16, but this is expected due to the much larger set of EOSs considered here. Note also that the difference between the PDFs obtained when imposing and not imposing the pQCD constraints is small but significant and has a clear physical origin, which we discuss below. More importantly, the new quasi-universal relations are slightly but systematically larger than those reported in BR16 and, indeed, the median of the latter falls outside the 95% confidence interval for both the ensembles with and without pQCD constraints. This is best seen in the right panel of Figure 2, which reports the one-dimensional PDFs of $M_{\rm crit}/M_{\rm TOV}$ at $j = j_{\rm Kep}$, i.e., the PDFs of $\mathcal{R}$. The medians of these PDFs are marked with red/blue dashed lines for EOSs built with/without the pQCD constraints, and while they differ by only $\simeq$1%, they are clearly separated. The reason for this is that the pQCD constraint leads to a softening of the EOS at large densities and, as a result, to smaller values of $M_{\rm TOV}$. Because the central density in maximally rotating stars is smaller than in TOV stars, the impact on $M_{\rm max}$ is also smaller; the combination of the two trends drives $\mathcal{R}$ toward slightly larger values. Finally, and more importantly, when considering the PDF obtained with the pQCD constraint being imposed, we can extract a new estimate for the mass ratio $\mathcal{R} = 1.255^{+0.047}_{-0.040}$, which is therefore $\simeq$4% larger than the estimate of BR16, who employed EOSs not satisfying the perturbative QCD constraint at high densities and

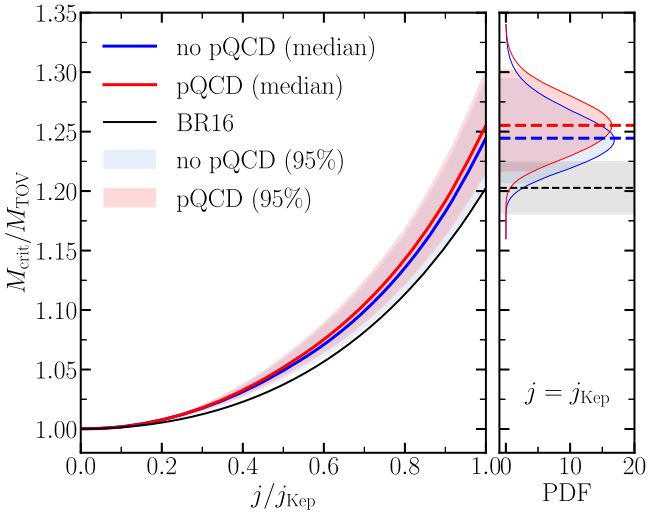

Figure 2. Left: quasi-universal relation of the gravitational mass along the critical line. Red-shaded (blue-shaded) areas indicate the 95% confidence intervals with (without) the pQCD constraint, while the solid lines mark the corresponding median values. The black solid line reports the prediction by Breu & Rezzolla (BR16). Right: one-dimensional slice of the PDFs for $j = j_{\rm Kep}$.

also a smaller value of $M_{\rm TOV}^{(-)}$ as deduced from the astrophysical constraints in 2016. Both of these conditions systematically lower the value of $\mathcal{R}$ (see also discussion below).

While the quasi-universality of the mass ratio $\mathcal{R}$ is robust, it is clear that the constraints imposed on the EOS ensemble will influence this ratio. To quantify this dependence, we also compute $\mathcal{R}$ for a smaller ($M_{\rm TOV}^{(-)} = 2.0\,M_\odot$) and a larger ($M_{\rm TOV}^{(-)} = 2.35\,M_\odot$) lower bound on $M_{\rm TOV}$. The results are reported in Table 1 [5] and show that the median of the PDF of $\mathcal{R}$ increases monotonically with the imposed lower bound on $M_{\rm TOV}$. Stated differently, imposing a larger cutoff on the TOV mass in the EOS ensemble drives the posterior for $M_{\rm max}$ upwards faster than that for $M_{\rm TOV}$. While this might seem counterintuitive at first, it is simple to understand. We recall that imposing larger bounds on $M_{\rm TOV}$ leads to a significant stiffening of the EOSs, i.e., in the energy-density range $0.5 < e/(\mathrm{GeV\,fm^{-3}}) < 0.8$ (see Figure 1 of Ecker & Rezzolla 2023) which is relevant for the cores of rapidly rotating stars. At the same time, such bounds have a negligible impact on energies $e \approx 1\,\mathrm{GeV\,fm^{-3}}$, which are those relevant for the cores of nonrotating stars (Altiparmak et al. 2022). This increase in $M_{\rm max}$ not being balanced by an equal increase in $M_{\rm TOV}$ leads to the measured growth of $\mathcal{R}$ with $M_{\rm TOV}^{(-)}$.

The new and more accurate estimate of $\mathcal{R}$ provides two important tools to be employed when a binary neutron-star merger is detected together with its electromagnetic counterpart. First, as discussed by Rezzolla et al. (2018b) in the case of GW170817, the detection of a gamma-ray burst counterpart following a binary neutron-star merger can be taken as indirect evidence for the formation of a black hole from the remnant and the emergence of a relativistic jet from the ejected matter (Gill et al. 2019). This implies that the mass of the merger remnant, properly reduced by the ejected rest mass and the mass lost in gravitational waves, is very close to $M_{\rm max}$, setting an upper limit for it. In turn, making use of $\mathcal{R}$, this can be used to set an upper limit on $M_{\rm TOV}$. Following this logic and employing the iterative procedure to account for an adaptive adjustment of the mass ratio (see Appendix for details), we obtain the following upper limit for the maximum mass: $M_{\rm TOV}^{(+)} = 2.24^{+0.07}_{-0.11}\,M_\odot$ with corresponding ratio $\mathcal{R} = 1.236^{+0.065}_{-0.036}$. Clearly, the same method can be employed to further refine the estimate of $M_{\rm TOV}^{(+)}$ as new detections of merging binary neutron-star systems are made.

A second consequence of the new estimate of $\mathcal{R}$ follows from the discussion in Most et al. (2020). In particular, once a gravitational-wave merger event with a significant mass difference, such as GW190814, is detected, knowledge of the total mass of the system and of the universal mass ratio $\mathcal{R}$ allows one to set constraints on the spin of the secondary (see Figure 1 of Most et al. 2020). More specifically, assuming that the secondary of GW190814 was a neutron star at the merger (see Nathanail et al. 2021, for a different conclusion), we can employ the new value of $\mathcal{R}$ to improve the constraints on the dimensionless spin of the secondary in GW190814 to be $0.52 \lesssim \chi_2 \lesssim 0.72$. Also in this case, the methodology discussed above can be applied to new detections of binaries with small mass ratios.

We next employ our large set of rotating-star models to assess the validity of other quasi-universal relations, and we start by reporting a novel quasi-universal relation found for the surface oblateness, i.e., the ratio between the polar and equatorial proper radii, $R_{\rm p}/R_{\rm e}$, along the critical line. This ratio is obviously unity in the case of nonrotating stars and decreases as the angular momentum is increased, since the equatorial radius becomes larger and the quadrupolar deformation of the star increases (see also Frieben & Rezzolla 2012; Konstantinou & Morsink 2022; Gao et al. 2023, for different but equally interesting relations). The result of our analysis in this case is presented in Figure 3, which is logically similar to Figure 2, but now for the ratio $R_{\rm p}/R_{\rm e}$. Interestingly, the quasi-universal relation has an extremely small variance, and this is most probably due to the fact that $R_{\rm p}/R_{\rm e}$ depends most sensitively on the low-density part of the EOSs, which is rather well constrained. This hypothesis is also corroborated by the fact that the result for this relation seems to be essentially independent of whether or not the perturbative QCD constraint is imposed, implying that the high-density portion of the EOS, where this constraint has an impact, is not involved in the deformation seen in Figure 3. Given the simple behavior of the relation, the corresponding medians can be very accurately described by a second-order polynomial of the form $R_{\rm p}/R_{\rm e} = 1 - b_2\,(j/j_{\rm Kep})^2$, and the corresponding best-fit coefficients are reported in Table 1 of the Appendix. The relevance of this result is that it allows for a much more accurate modeling of the emission from rotating neutron stars, such as those observed by NICER, where a precise knowledge of the surface deformation is essential for the modeling of the X-ray emission from the hot spots of rotating stars (Morsink et al. 2007; Bogdanov et al. 2019), although it is important to keep in mind that the results presented in this work only apply to systems that are close to the critical mass. Furthermore, it can be employed when studying high-mass black-widow systems, where rapid rotation is expected and indeed observed (with a spin frequency of $f = 706$ Hz, PSR J0952-0607 is the second-fastest-spinning pulsar known (Romani et al. 2022) and has $j/j_{\rm Kep} \lesssim 0.46$).

[5] Given the rapid convergence of the PDFs with the number of EOSs (see Appendix), we have considered 10^4 EOSs for these different bounds.

Table 1
Estimates for Various Properties of Static and Rotating Neutron Stars

$M_{\rm TOV}^{(-)}$ ($M_\odot$)	pQCD	$\mathcal{R}$	a_2	b_2	$c^2_{s,{\rm c,Kep}}$	$c^2_{s,{\rm c,TOV}}$	$\Delta_{\rm c,Kep}$	$\Delta_{\rm c,TOV}$	$d_{\rm c,Kep}$	$d_{\rm c,TOV}$
2.00	yes	$1.248^{+0.054}_{-0.043}$	$0.18^{+0.04}_{-0.02}$	$0.41^{+0.02}_{-0.02}$	$0.245^{+0.381}_{-0.195}$	$0.208^{+0.369}_{-0.172}$	$0.031^{+0.115}_{-0.136}$	$0.038^{+0.117}_{-0.133}$	$0.118^{+0.209}_{-0.095}$	$0.130^{+0.180}_{-0.102}$
	no	$1.240^{+0.055}_{-0.043}$	$0.16^{-0.04}_{-0.02}$	$0.40^{+0.03}_{-0.02}$	$0.377^{+0.491}_{-0.316}$	$0.348^{+0.502}_{-0.306}$	$-0.024^{+0.159}_{-0.162}$	$-0.031^{+0.143}_{-0.174}$	$0.146^{+0.286}_{-0.117}$	$0.153^{+0.260}_{-0.124}$
2.20	yes	$1.255^{+0.047}_{-0.040}$	$0.18^{+0.03}_{-0.02}$	$0.41^{+0.02}_{-0.02}$	$0.248^{+0.388}_{-0.195}$	$0.201^{+0.360}_{-0.167}$	$0.017^{+0.104}_{-0.129}$	$0.029^{+0.108}_{-0.133}$	$0.114^{+0.214}_{-0.094}$	$0.135^{+0.180}_{-0.107}$
	no	$1.244^{+0.050}_{-0.039}$	$0.17^{-0.04}_{-0.02}$	$0.40^{+0.02}_{-0.02}$	$0.398^{+0.470}_{-0.325}$	$0.365^{+0.489}_{-0.314}$	$-0.038^{+0.147}_{-0.153}$	$-0.046^{+0.167}_{-0.166}$	$0.146^{+0.288}_{-0.120}$	$0.156^{+0.260}_{-0.126}$
2.35	yes	$1.260^{+0.041}_{-0.034}$	$0.18^{-0.03}_{-0.02}$	$0.41^{+0.02}_{-0.02}$	$0.256^{+0.386}_{-0.198}$	$0.195^{+0.326}_{-0.164}$	$0.003^{+0.094}_{-0.121}$	$0.019^{+0.100}_{-0.129}$	$0.112^{+0.222}_{-0.093}$	$0.138^{+0.180}_{-0.110}$
	no	$1.248^{+0.046}_{-0.034}$	$0.16^{-0.04}_{-0.02}$	$0.40^{+0.02}_{-0.01}$	$0.419^{+0.458}_{-0.338}$	$0.375^{+0.487}_{-0.322}$	$-0.052^{+0.137}_{-0.142}$	$-0.059^{+0.162}_{-0.158}$	$0.152^{+0.285}_{-0.126}$	$0.161^{+0.263}_{-0.131}$

Note. The central values and the uncertainties correspond to the median and the 95% confidence intervals of the PDF, respectively. Note that the upper and lower bounds of a_2 have been computed with (1) using the corresponding upper and lower bounds of $\mathcal{R}$.

Finally, we use our EOS ensemble to assess the validity of the so-called "*I*–*Q*" quasi-universal relations, where I is the stellar moment of inertia and Q the mass quadrupole moment. The IQ relations were first investigated by Yagi & Yunes (2013) in the context of slowly rotating neutron stars and subsequently extended to stars in rapid rotation by Chakrabarti et al. (2014), Doneva et al. (2014), and Pappas & Apostolatos (2014). The last of these, in particular, has found quasi-universal relations between I and Q also for rapidly rotating stars and expressed them in terms of j. Since these functions were validated using a dozen nuclear-physics EOSs only, it is interesting and important to assess the validity of such relations when employing a much larger set of model-independent EOSs (see also Nath et al. 2023, for similar recent work). Overall, we find that the fit proposed by Pappas & Apostolatos (2014) performs very well also with the much larger ensemble of EOSs, and the differences in the newly estimated best-fit coefficients are of the order of 1%, with the largest differences of ∼2.5% being attained in the low-Q and high-j region of the parameter space (see Appendix for details).

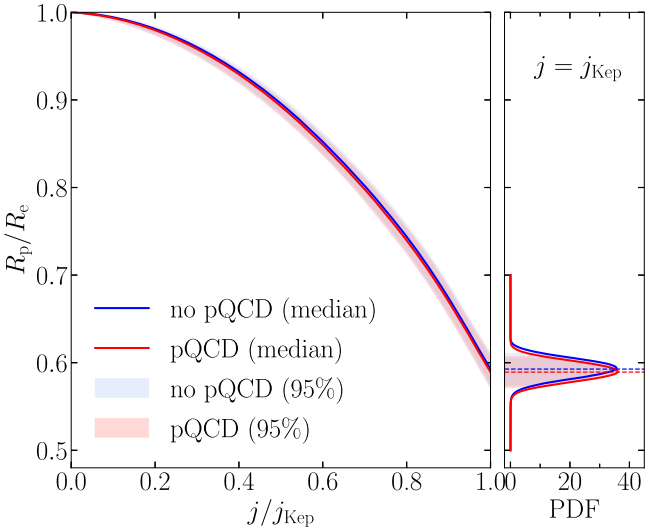

Figure 3. The same as in Figure 2 but for the novel quasi-universal relation for the ratio of the polar and equatorial radii along the critical line.

4. Conclusion

Motivated by recent advances in model-agnostic sampling methods for the EOS of neutron-star matter (Kurkela et al. 2014; Lattimer & Steiner 2014; Tews et al. 2018a; Most et al. 2018; Steiner et al. 2018; Annala et al. 2020; Altiparmak et al. 2022), we have revisited the quasi-universal behavior of isolated rotating and nonrotating neutron stars by employing a very large sample of generic EOSs constructed with a 10-segment parameterization of the sound speed (Annala et al. 2020; Altiparmak et al. 2022). By exploring the whole physically allowed space of solutions, our approach has the advantage of being able to test rigorously whether a quasi-universality is present or not and to study the dependence of the quasi-universal behavior on the imposed constraints.

Our attention here has been focused on the quasi-universal relation of the mass along the critical line and, more particularly, on the mass ratio $\mathcal{R}$ between the maximum masses of rotating and nonrotating stars (Breu & Rezzolla 2016). Our analysis has revealed that such a relation is still valid when considering an ensemble of up to 10^6 EOSs obtained when either imposing or not the constraints from pQCD at high densities, and with different lower bounds the maximum mass of nonrotating stars $M_{\rm TOV}$. While the variance in the new estimates is comparable to but larger than that in BR16, the median values are a few percent larger than the original estimate of BR16. This is not surprising given the comparatively small number of EOSs considered by BR16. Furthermore, we have found that increasing the lower bound on $M_{\rm TOV}$ also leads to a larger value of $\mathcal{R}$, while neglecting the pQCD constraints at high densities leads to a decrease in this ratio.

Finally, we have employed our large set of EOSs to assess the validity of known and novel quasi-universal relations. In particular, we have revealed the existence of a new and tight quasi-universal relation for the surface oblateness, which can be used to model more accurately the emission from the hot spots on the surface of rotating neutron stars, such as those observed by NICER. At the same time, we were able to confirm the validity of the *I*–*Q* relations over a broad range of rotations, from slow rotation up to the mass-shedding limit, and to improve the best-fit coefficients of the functional behavior proposed by Pappas & Apostolatos (2014) in the low-Q and high-j region of the parameter space.

Besides improving previously known results, and although not obtained from a fully Bayesian analysis, the more accurate estimate of $\mathcal{R}$ offers two important and direct applications whenever a binary neutron-star merger is detected together with its electromagnetic counterpart. In particular, it can be used to set new and tighter constraints on the maximum mass of nonrotating stars and hence on the EOS. For example, when considering GW170817, this implies a new upper limit of $M_{\rm TOV}^{(+)} = 2.24^{+0.07}_{-0.11}\ M_\odot$, although it should be noted that the

error bars for $M_{\rm TOV}^{(+)}$ might be underestimated due to the fact that the result was not marginalized over the prior for $M_{\rm TOV}^{(-)}$. Furthermore, in binaries with small mass ratio it can be employed to set constraints on the dimensionless spin of the secondary object when this is represented by a neutron star. For example, when considering the case of GW190814, the new value of $\mathcal{R}$ implies a new bracketing interval of $0.52 \lesssim \chi_2 \lesssim 0.72$. The present data-taking runs of the LIGO–Virgo–Kagra collaboration will hopefully provide us with a number of potential applications of these findings.

Acknowledgments

We are grateful to R. Duqué and T. Gorda for insightful discussions and comments. We also thank R. Mallick for his careful reading of the manuscript. Partial funding comes from the State of Hesse within the Research Cluster ELEMENTS (Project ID 500/10.006), by the ERC Advanced Grant "JETSET: Launching, propagation and emission of relativistic jets from binary mergers and across mass scales" (grant No. 884631). C.E. acknowledges support by the Deutsche Forschungsgemeinschaft (DFG, German Research Foundation) through the CRC-TR 211 "Strong-interaction matter under extreme conditions"—project number 315477589—TRR 211. L.R. acknowledges the Walter Greiner Gesellschaft zur Förderung der physikalischen Grundlagenforschung e.V. through the Carl W. Fueck Laureatus Chair. The calculations were performed on the local ITP Supercomputing Clusters Iboga and Calea.

Data Availability

Data are available upon reasonable request from the corresponding author.

Appendix

A.1. Overview of the Stellar Properties

In Figure 4 we show the PDFs for the EOSs (left panels) and the corresponding mass–radius relation of static (middle panels) and maximally rotating stars (right panels) when imposing (top row) or not (bottom row) the pQCD constraint and assuming $M_{\rm TOV}^{(-)} = 2.2\,M_\odot$. As clearly shown by the figure, the allowed pressure band is influenced by imposing the pQCD constraint down to energy densities $e \sim 800\,{\rm MeV\,fm^{-3}}$, which are relevant for the cores of heavy nonrotating TOV stars and even for rapidly rotating stars. In particular, the EOSs are allowed to be significantly stiffer and with higher sound speeds (i.e., with steeper curves in the (p, e) space) in the range 0.8–1.2 GeV fm^{-3} since the EOSs do not need to be causally connected to the pQCD band at high densities. As can be observed in the two rightmost columns of Figure 4, and in Figure 1, the effect of this stiffening in the intermediate- to high-density regime is to allow for higher masses and to increase the radii of stars close to the stability limit. In particular, the lower panels in these figures show that the distributions of radii for $1.4\,M_\odot$ models vary only modestly whether or not the EOS ensemble is restricted to being compatible with the results of pQCD. On the other hand, the contours of the distribution close to the critical limit clearly show that the constraint has a non-negligible impact on TOVs (which was already shown in Gorda et al. 2023a), as well as on rapidly rotating stars, which we show here for the first time.

Similarly, in Figure 5 we report the one-dimensional PDFs for the sound speed (left column), for the normalized trace anomaly $\Delta = 1/3 - p/e$ (Fujimoto et al. 2022) (middle column), and for the measure of the non-conformality of the matter $d_c := \sqrt{\Delta^2 + (\Delta')^2}$ (right column), where Δ' is the logarithmic derivative of Δ with respect to the energy density. All quantities are computed at the center of stellar models with $j = 0$ (top row) and $j = j_{\rm Kep}$ (bottom row). The median values, together with the 95% error bars, are reported in Table 1. Overall, our results compare well with the corresponding slices calculated by Annala et al. (2023), as well as with the results of Gorda et al. (2023a), obtained with a Gaussian process regression technique (Landry & Essick 2019).

Finally, in Table 1 we also report the median values with 95% error bars for $\mathcal{R}$, the best-fit value for the coefficient a_2, the central sound speed squared in either maximally rotating ($c^2_{s,{\rm c,Kep}}$) or static stars ($c^2_{s,{\rm c,TOV}}$). The last four columns report the central values of the conformal anomaly Δ_c and d_c for various choices of $M_{\rm TOV}^{(-)}$, and with or without imposing the pQCD constraint.

A.2. Convergence and an Upper Bound on $M_{\rm TOV}$

To demonstrate the robustness and convergence of the results for $\mathcal{R}$ obtained with our sampling procedure we compare in Figure 6 the one-dimensional PDFs obtained with our procedure for the ratio $\mathcal{R}$; obviously, this is the same as showing the distribution of $M_{\rm crit}/M_{\rm TOV}$ for $j = j_{\rm Kep}$ as done in Figure 2. As can be readily observed, the median of our results is surprisingly robust even when only 10^2 EOSs are used, and the corresponding median value is well within 1σ away from the result obtained with 10^6 EOSs. This notwithstanding, the overall behavior of the PDF can be seen to be significantly more noisy for the cases with lower statistics, and, in particular, far fewer EOSs sample the tails of the distribution. For this reason, it is still important to use large statistics so that the 100% confidence interval can be trusted to span the whole physically allowed region for $\mathcal{R}$.

Next, we discuss how to obtain a new upper limit of the maximum mass of nonrotating stars after using the newly estimate for $\mathcal{R}$ and the assumption that the GW170817 remnant collapsed while still rotating at a frequency close to the mass-shedding limit. Under these assumptions, it is possible to obtain a first rough upper bound on $M_{\rm TOV}$ by simply observing that $M_{\rm max} < M_{\rm GW170817} = 2.74^{+0.04}_{-0.01}\,M_\odot$, and by subsequently using the value of $\mathcal{R} := M_{\rm max}/M_{\rm TOV}$ obtained by the quasi-universal relation presented in the main text. This estimate can be further refined by making use of the iterative procedure outlined below.

1. We construct an EOS ensemble as discussed in the main text, recalling that the dependence of $\mathcal{R}$ on the lower bound imposed on $M_{\rm TOV}$ is weak but non-negligible (we here set of $M_{\rm TOV}^{(-)} = 2.08\,M_\odot$).
2. We determine the quasi-universal ratio $\mathcal{R}^{n=1}$, where n is the iteration number.
3. Assuming that GW170817 collapsed to a black hole, we determine the upper bound $M_{\rm TOV}^{(+)}$.
4. We construct a new ensemble of EOSs, but this time imposing as upper bound on $M_{\rm TOV}$ the value determined in point 3.

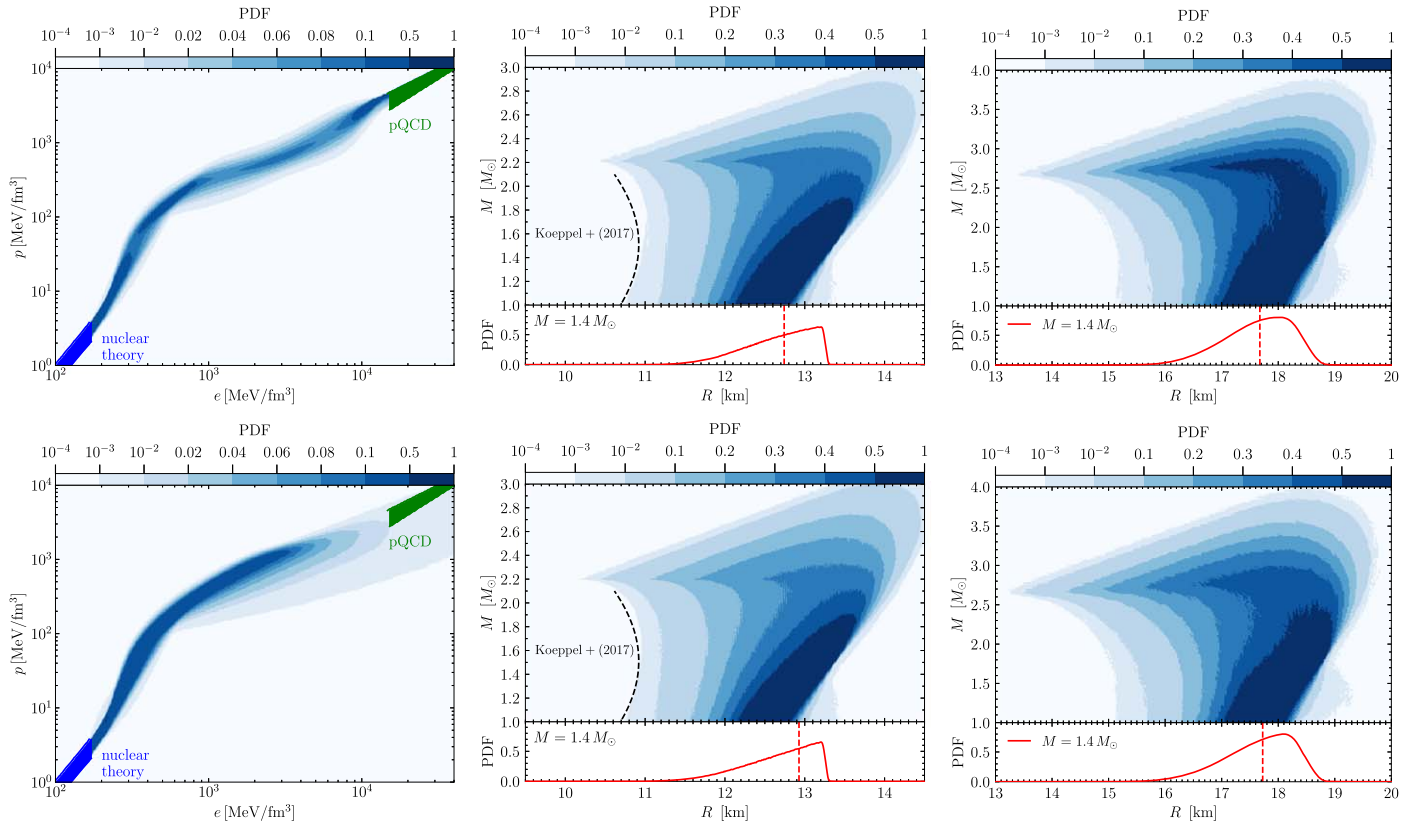

Figure 4. PDFs of the EOSs (left panels), of the mass–radius relation of nonrotating stars (middle panels), and of stars rotating at the mass-shedding frequency (right panels). The top and bottom rows refer, respectively, to ensembles where the pQCD constraints are imposed or not; in all cases $M_{\rm TOV}^{(-)} = 2.2\ M_\odot$.

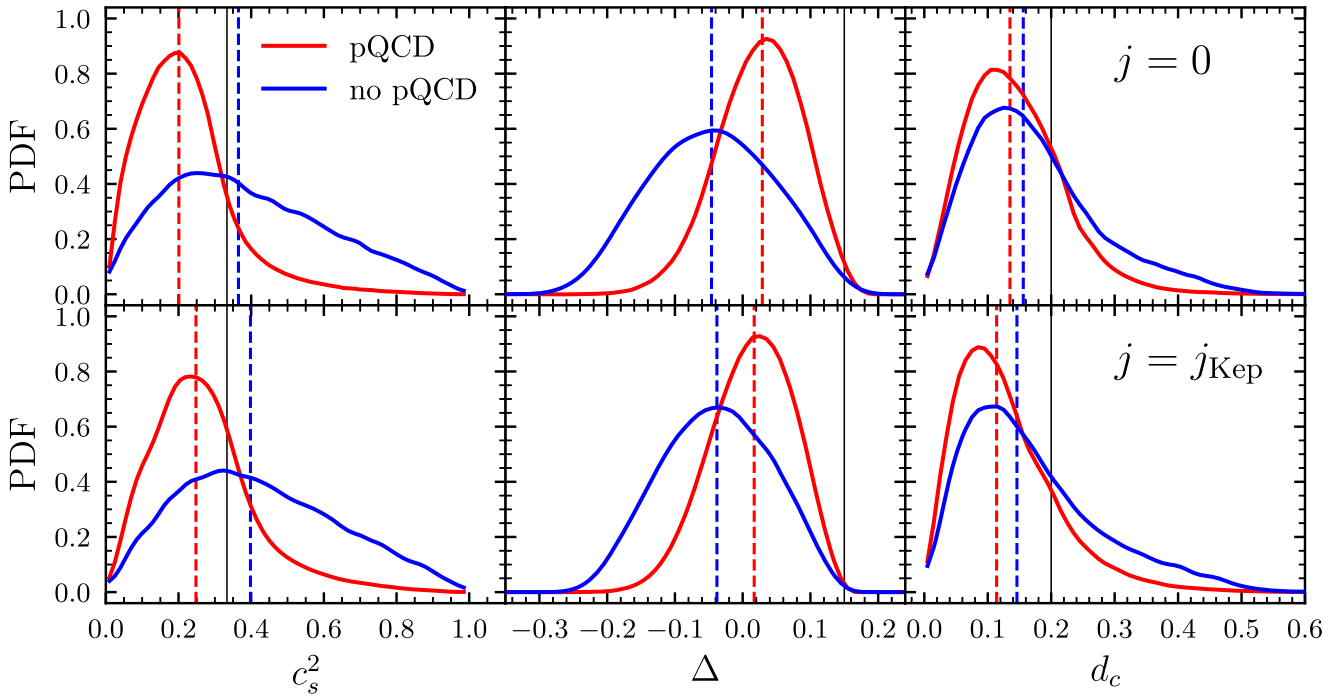

Figure 5. One-dimensional PDFs for the sound speed (left column), for the normalized trace anomaly (middle column), and for the measure of the non-conformality of the matter (right column). All quantities are computed at the center of stellar models with $j = 0$ (top row) and $j = j_{\rm Kep}$ (bottom row). Vertical black lines are approximate upper bounds reported in Annala et al. (2023) for quark matter in pQCD at $n_b > 40 n_s$.

Table 2
Best-fit Coefficients for the I–Q Quasi-universal Relation Proposed by Pappas & Apostolatos (2014) (see Equation (A1)) with $M_{\rm TOV}^{(-)} = 2.2\,M_\odot$

pQCD	A_1	B_1	B_2	B_3	C_1	C_2	C_3	ξ_0
Yes	2.07	0.764	0.238	0.816	0.143	0.0316	−0.128	0.908
No	2.12	0.705	0.537	0.519	0.175	−0.100	0.014	0.951

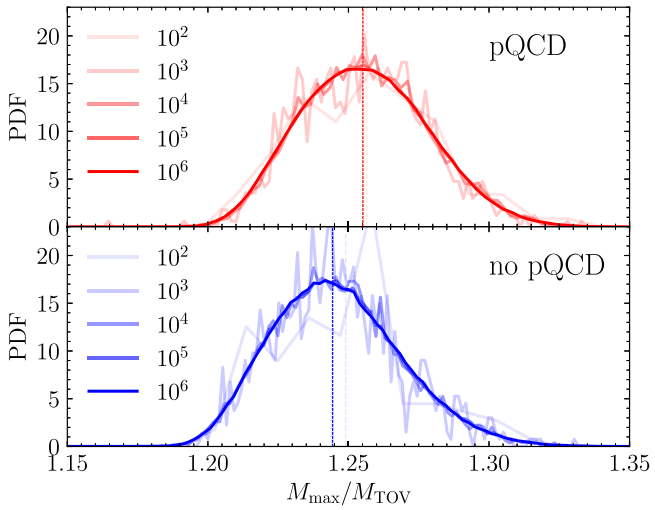

Figure 6. One-dimensional PDFs of $\mathcal{R}$ when varying the number of EOSs in the set assuming $M_{\rm TOV} > 2.2\,M_\odot$. Note that 10^3 EOSs are already sufficient to obtain a very small variance.

5. We recompute $\mathcal{R}^n$ and keep iterating from point 3 until convergence has been reached. We find that $n = 3$ is sufficient to obtain differences below 1% between $\mathcal{R}^n$ and $\mathcal{R}^{n+1}$.

Following this iterative procedure we have derived the converged upper limit for the maximum mass of nonrotating neutron stars when imposing the pQCD constraint and the corrsponding value for $\mathcal{R}$ reported in the main text: $M_{\rm TOV}^{(+)} = 2.24^{+0.07}_{-0.11}\ M_\odot$, $\mathcal{R} = 1.236^{+0.065}_{-0.036}$.

A.3. Quasi-universal Relations for Rapidly Rotating Stars

Following Pappas & Apostolatos (2014), we define the dimensionless moment of inertia and quadrupole, respectively, as $\bar{I} := I/M^3$ and $\bar{Q}$: $=Q/(M^3 j^2)$, and seek a quasi-universal expression for $\bar{I}$ as a function of j and $\bar{Q}$ via the ansatz

$$\sqrt{\bar{I}} = A_1 + A_2(\sqrt{\bar{Q}} - \xi_0) + A_3(\sqrt{\bar{Q}} - \xi_0)^2, \qquad \text{(A1)}$$

where

$$A_2 := B_1 + B_2\, j + B_3\, j^2 \quad \text{and} \quad A_3 := C_1 + C_2\, j + C_3\, j^2, \qquad \text{(A2)}$$

with A_1, B_1–B_3, C_1–C_3, and ξ_0 as fitting parameters. The corresponding values for the EOS ensembles with $M_{\rm TOV}^{(-)} = 2.2\,M_\odot$ and when the pQCD constraints are taken into account or not are reported in Table 2.

ORCID iDs

Carlo Musolino https://orcid.org/0000-0002-9955-3451
Christian Ecker https://orcid.org/0000-0002-8669-4300
Luciano Rezzolla https://orcid.org/0000-0002-1330-7103

References

Altiparmak, S., Ecker, C., & Rezzolla, L. 2022, ApJL, 939, L34
Annala, E., Gorda, T., Hirvonen, J., et al. 2023, NatCo, 14, 8451
Annala, E., Gorda, T., Katerini, E., et al. 2022, PhRvX, 12, 011058
Annala, E., Gorda, T., Kurkela, A., Nättilä, J., & Vuorinen, A. 2020, NatPh, 16, 907
Bastian, N.-U. F. 2021, PhRvD, 103, 023001
Bauswein, A., Bastian, N.-U. F., Blaschke, D. B., et al. 2019, PhRvL, 122, 061102
Bauswein, A., & Janka, H.-T. 2012, PhRvL, 108, 011101
Beloin, S., Han, S., Steiner, A. W., & Odbadrakh, K. 2019, PhRvC, 100, 055801
Bernuzzi, S., Nagar, A., Balmelli, S., Dietrich, T., & Ujevic, M. 2014, PhRvL, 112, 201101
Bogdanov, S., Lamb, F. K., Mahmoodifar, S., et al. 2019, ApJL, 887, L26
Bozzola, G., Espino, P. L., Lewin, C. D., & Paschalidis, V. 2019, EPJA, 55, 149
Brandes, L., Weise, W., & Kaiser, N. 2023, PhRvD, 108, 094014
Breu, C., & Rezzolla, L. 2016, MNRAS, 459, 646
Chakrabarti, S., Delsate, T., Gürlebeck, N., & Steinhoff, J. 2014, PhRvL, 112, 201102
Cook, G. B., Shapiro, S. L., & Teukolsky, S. A. 1994a, ApJ, 422, 227
Cook, G. B., Shapiro, S. L., & Teukolsky, S. A. 1994b, ApJ, 424, 823
Demircik, T., Ecker, C., & Järvinen, M. 2021, ApJL, 907, L37
Demircik, T., Ecker, C., & Järvinen, M. 2022, PhRvX, 12, 041012
Doneva, D. D., Yazadjiev, S. S., Stergioulas, N., & Kokkotas, K. D. 2014, ApJL, 781, L6
Drischler, C., Melendez, J. A., Furnstahl, R. J., & Phillips, D. R. 2020, PhRvC, 102, 054315
Ecker, C., & Rezzolla, L. 2022, ApJL, 939, L35
Ecker, C., & Rezzolla, L. 2023, MNRAS, 519, 2615
Fonseca, E., et al. 2021, ApJL, 915, L12
Freedman, B. A., & McLerran, L. D. 1977, PhRvD, 16, 1169
Frieben, J., & Rezzolla, L. 2012, MNRAS, 427, 3406
Friedman, J. L., Ipser, J. R., & Sorkin, R. D. 1988, ApJ, 325, 722
Fujimoto, Y., Fukushima, K., McLerran, L. D., & Praszalowicz, M. 2022, PhRvL, 129, 252702
Gandolfi, S., Lippuner, J., Steiner, A. W., et al. 2019, JPhG, 46, 103001
Gao, Y., Shao, L., & Steinhoff, J. 2023, ApJ, 954, 16
Gill, R., Nathanail, A., & Rezzolla, L. 2019, ApJ, 876, 139
Gonzalez, A., Zappa, F., Breschi, M., et al. 2023, CQGra, 40, 085011
Gorda, T., Komoltsev, O., & Kurkela, A. 2023a, ApJ, 950, 107
Gorda, T., Komoltsev, O., Kurkela, A., & Mazeliauskas, A. 2023b, JHEP, 2023, 2
Gorda, T., Kurkela, A., Paatelainen, R., Säppi, S., & Vuorinen, A. 2021a, PhRvD, 104, 074015
Gorda, T., Kurkela, A., Paatelainen, R., Säppi, S., & Vuorinen, A. 2021b, PhRvL, 127, 162003
Haskell, B., Ciolfi, R., Pannarale, F., & Rezzolla, L. 2014, MNRAS, 438, L71
Hebeler, K., Lattimer, J. M., Pethick, C. J., & Schwenk, A. 2013, ApJ, 773, 11
Ivanytskyi, O., & Blaschke, D. 2022, EPJA, 58, 152
Jiang, J.-L., Ecker, C., & Rezzolla, L. 2023, ApJ, 949, 11
Jie, Li, J., Sedrakian, A., & Alford, M. 2021, PhRvD, 104, L121302
Jie, Li, J., Sedrakian, A., & Weber, F. 2023, PhRvC, 108, 025810
Keller, J., Wellenhofer, C., Hebeler, K., & Schwenk, A. 2021, PhRvC, 103, 055806
Khosravi Largani, N., Fischer, T., Sedrakian, A., et al. 2022, MNRAS, 515, 3539
Koeppel, S., Bovard, L., & Rezzolla, L. 2019, ApJL, 872, L16
Komoltsev, O., & Kurkela, A. 2022, PhRvL, 128, 202701
Konstantinou, A., & Morsink, S. M. 2022, ApJ, 934, 139
Kurkela, A., Fraga, E. S., Schaffner-Bielich, J., & Vuorinen, A. 2014, ApJ, 789, 127
Landry, P., & Essick, R. 2019, PhRvD, 99, 084049
Lasota, J.-P., Haensel, P., & Abramowicz, M. A. 1996, ApJ, 456, 300

Lattimer, J. M., & Steiner, A. W. 2014, ApJ, 784, 123
Marczenko, M., McLerran, L., Redlich, K., & Sasaki, C. 2023, PhRvC, 107, 025802
Margalit, B., & Metzger, B. D. 2017, ApJL, 850, L19
Miller, M. C., Lamb, F. K., Dittmann, A. J., et al. 2019, ApJL, 887, L24
Miller, M. C., Lamb, F. K., Dittmann, A. J., et al. 2021, ApJL, 918, L28
Morsink, S. M., Leahy, D. A., Cadeau, C., & Braga, J. 2007, ApJ, 663, 1244
Most, E. R., Papenfort, L. J., Dexheimer, V., et al. 2019, PhRvL, 122, 061101
Most, E. R., Papenfort, L. J., Weih, L. R., & Rezzolla, L. 2020, MNRAS, 499, L82
Most, E. R., Weih, L. R., Rezzolla, L., & Schaffner-Bielich, J. 2018, PhRvL, 120, 261103
Nath, K., Mallick, R., & Chatterjee, S. 2023, MNRAS, 524, 1438
Nathanail, A., Most, E. R., & Rezzolla, L. 2021, ApJL, 908, L28
Pappas, G., & Apostolatos, T. A. 2014, PhRvL, 112, 121101
Read, J. S., Baiotti, L., Creighton, J. D. E., et al. 2013, PhRvD, 88, 044042
Read, J. S., Lackey, B. D., Owen, B. J., & Friedman, J. L. 2009, PhRvD, 79, 124032
Rezzolla, L., Most, E. R., & Weih, L. R. 2018a, ApJL, 852, L25
Rezzolla, L., Pizzochero, P., Jones, D. I., Rea, N., & Vidaña, I. 2018b, The Physics and Astrophysics of Neutron Stars, Vol. 457 (Cham: Springer)
Rezzolla, L., & Takami, K. 2016, PhRvD, 93, 124051
Riley, T. E., Watts, A. L., Bogdanov, S., et al. 2019, ApJL, 887, L21
Riley, T. E., Watts, A. L., Ray, P. S., et al. 2021, ApJL, 918, L27
Romani, R. W., Kandel, D., Filippenko, A. V., Brink, T. G., & Zheng, W. 2022, ApJL, 934, L18
Ruiz, M., Shapiro, S. L., & Tsokaros, A. 2018, PhRvD, 97, 021501
Shibata, M., Zhou, E., Kiuchi, K., & Fujibayashi, S. 2019, PhRvD, 100, 023015
Steiner, A. W., Heinke, C. O., Bogdanov, S., et al. 2018, MNRAS, 476, 421
Stergioulas, N., & Friedman, J. L. 1995, ApJ, 444, 306
Takami, K., Rezzolla, L., & Baiotti, L. 2015, PhRvD, 91, 064001
Takami, K., Rezzolla, L., & Yoshida, S. 2011, MNRAS, 416, L1
Tews, I., Carlson, J., Gandolfi, S., & Reddy, S. 2018a, ApJ, 860, 149
Tews, I., Margueron, J., & Reddy, S. 2018b, PhRvC, 98, 045804
The LIGO Scientific Collaboration, the Virgo Collaboration, Abbott, B. P., et al. 2019, PhRvX, 9, 011001
Traversi, S., Char, P., & Pagliara, G. 2020, ApJ, 897, 165
Vuorinen, A. 2003, PhRvD, 68, 054017
Weih, L. R., Hanauske, M., & Rezzolla, L. 2020, PhRvL, 124, 171103
Weih, L. R., Most, E. R., & Rezzolla, L. 2018, MNRAS, 473, L126
Yagi, K., & Yunes, N. 2013, Sci, 341, 365
Yagi, K., & Yunes, N. 2017, PhR, 681, 1